Replication protein A associates with nucleolar R loops and regulates rRNA transcription and nucleolar morphology

Shuang Feng and James L. Manley

Department of Biological Sciences, Columbia University, New York, New York 10027, USA

The nucleolus is an important cellular compartment in which ribosomal RNAs (rRNAs) are transcribed and where certain stress pathways that are crucial for cell growth are coordinated. Here we report novel functions of the DNA replication and repair factor replication protein A (RPA) in control of nucleolar homeostasis. We show that loss of the DNA:RNA helicase senataxin (SETX) promotes RPA nucleolar localization, and that this relocalization is dependent on the presence of R loops. Notably, this nucleolar RPA phenotype was also observed in the presence of camptothecin (CPT)-induced genotoxic stress, as well as in SETX-deficient AOA2 patient fibroblasts. Extending these results, we found that RPA is recruited to rDNA following CPT treatment, where RPA prevents R-loop-induced DNA double-strand breaks. Furthermore, we show that loss of RPA significantly decreased 47S pre-rRNA levels, which was accompanied by increased expression of both RNAP II-mediated "promoter and pre-rRNA antisense" RNA as well as RNAP I-transcribed intragenic spacer RNAs. Finally, and likely reflecting the above, we found that loss of RPA promoted nucleolar structural disorganization, characterized by the appearance of reduced size nucleoli. Our findings both indicate new roles for RPA in nucleoli through pre-rRNA transcriptional control and also emphasize that RPA function in nucleolar homeostasis is linked to R-loop resolution under both physiological and pathological conditions.

[*Keywords*: R loop; RNA polymerase I (RNAP I); RNaseH1; replication protein A (RPA); senataxin (SETX)]

Supplemental material is available for this article.

Received July 23, 2021; revised version accepted October 22, 2021.

Cotranscriptional R loops consist of RNA:DNA hybrids and ssDNA, and are formed when nascent RNA anneals to the template DNA strand. These structures can be found in all cells, prokaryotic and eukaryotic, and have been shown to contribute to cellular stress and to result in activation of the DNA damage response (DDR) (Li and Manley 2005; García-Muse and Aguilera 2019). Remarkably, in mammals R loops have been estimated to occupy as much as 5% of the genome (Sanz et al. 2016). They are abundant at gene promoter and terminator regions, and have been associated with epigenetic regulation (Ginno et al. 2012; Castellano-Pozo et al. 2013; Santos-Pereira and Aguilera 2015). Genome-wide studies have shown that R loops are also abundant at tRNA genes, retrotransposons, and rDNA and in mitochondrial DNA (El Hage et al. 2014). R loops can have important physiological functions, as initially observed in immunoglobulin class switch recombination (Daniels and Lieber 1995; Yu et al. 2003). Subsequently, it was observed that R loops can form during RNAP II transcription at G-rich pause sites located downstream from polyadenylation signals, and that these are resolved by SETX and the 5′-to-3′ exoribonuclease XRN2 as part of transcription termination (Skourti-Stathaki et al. 2011). SETX was also shown to interact with the nuclear exosome, a 3′-to-5′ exoribonuclease, functioning to facilitate R-loop removal at sites of transcription–replication complex collisions (Richard et al. 2013).

Even though R loops can play important physiological roles in cells, there is considerable evidence that inappropriate R-loop formation can be problematic as R loops can block efficient transcription and replication, triggering the DDR. Consistent with this, R-loop deregulation has been linked to a number of diseases (Sollier and Cimprich 2015; Richard and Manley 2017). For example, amyotrophic lateral sclerosis 4 (ALS4) and ataxia with ocular apraxia type 2 (AOA2) both arise from mutations in *SETX*, and defects in R-loop resolution have been implicated (Richard et al. 2013; Skourti-Stathaki and Proudfoot 2014). Indeed, AOA2 mutations in SETX disrupt the interaction with the exosome noted above (Richard et al. 2013). In addition, R loops have been linked with transcriptional

Corresponding author: jlm2@columbia.edu

Article published online ahead of print. Article and publication date are online at http://www.genesdev.org/cgi/doi/10.1101/gad.348858.121.

pausing in BRACA1- and BRCA2- associated breast cancers, suggesting possible roles in tumorigenesis (Bhatia et al. 2014; Hatchi et al. 2015; Stork et al. 2016).

Despite the emerging evidence showing the importance of R loops in pathological and physiological processes, how these structures might affect rRNA transcription in nucleoli, where R loops are abundant, is largely unknown. Sen1 (yeast SETX homolog), RNaseH1, and Topoisomerase I (Top 1) have been implicated in suppression of R loops in the nucleolus (Chan et al. 2014; Shen et al. 2017). Consistent with this, inhibition of Top1 by camptothecin (CPT) treatment was found to increase nucleolar R loops (Marinello et al. 2013; Shen et al. 2017). Furthermore, depletion of Top1 increases R-loop formation at rDNA 5′ETS (5′ external transcribed spacer) regions, suggesting a possible role in rRNA transcriptional control (Manzo et al. 2018). Notably, control of rRNA transcription can be affected by at least two other RNA-based mechanisms. In one, promoter RNAs (pRNAs) are transcribed by RNAP I from intergenic upstream spacer promoters (SPs) and extend across the rDNA upstream control element (UCE) and core promoter region, interact with chromatin remodeling factors, and negatively regulate rRNA transcription (Mayer et al. 2008; Wehner et al. 2014). Indeed, pRNAs also form RNA:DNA hybrids at the UCE region (Grummt and Längst 2013; Wehner et al. 2014). The formation of these hybrids may prevent binding of transcription factors to the rRNA promoter, thereby blocking RNAP I transcription (Santoro and Grummt 2001; Schmitz et al. 2010; Grummt and Längst 2013). A second RNA, "promoter and pre-rRNA antisense" (*PAPAS*), is a long noncoding RNA that is transcribed by RNAP II in an orientation antisense to pre-rRNA (Bierhoff et al. 2010). Recently, *PAPAS* was shown to function in tumor growth inhibition (Xiao et al. 2020), perhaps by recruiting the NuRD remodeling complex to rDNA promoters to repress rDNA transcription (Zhao et al. 2018). Notably, R loops have been found associated with antisense transcription throughout the genome, and removal of R loops by RNaseH1 overexpression can selectively eliminate antisense transcripts in yeast and humans (Chan et al. 2014; Tan-Wong et al. 2019).

Replication protein A (RPA) has also been suggested to function in R-loop resolution. RPA is a ssDNA binding heterotrimer—composed of RPA70, RPA32, and RPA14—that is well known to function in DNA replication and repair (Wold 1997). RPA can also function in transcription by interacting with transcription factors or RNAP II (Daniely and Borowiec 2000; Sikorski et al. 2011). Furthermore, RPA participates in R-loop resolution by associating with and recruiting RNaseH1 to sites of R-loop formation and enhancing RNaseH1 activity (Nguyen et al. 2017). It is also notable that RPA binds to nucleolin, which functions in ribosome biogenesis and RNAP I transcription (Cong et al. 2012). This interaction inhibits RPA activity and DNA replication in response to heat shock or genotoxic stress (Daniely and Borowiec 2000; Kim et al. 2005). Notably, SETX was also shown to interact with nucleolin (Suraweera et al. 2009) through its N-terminal protein interaction domain detected by coimmunoprecipitation, consistent with a possible nucleolar role. Given that RPA and SETX, have documented functions in R-loop resolution and interact with nucleolin, an important question is whether these two factors function in R-loop metabolism in the nucleolus, especially in response to stress.

In this study, we have investigated how RPA and SETX functionally interact. Our data show that when SETX levels are reduced by depletion or in AOA2 patient cells, RPA accumulates in nucleoli, and it does so also following genotoxic stress induced by CPT treatment. This relocalization occurs in response to R-loop formation, and we show that loss of RPA results in increased accumulation of R loops across rDNA loci. Levels of 47S pre-rRNA decline under these conditions, perhaps as a result of elevated pRNA and *PAPAS* expression and accompanying sense and antisense R-loop formation. These changes in nucleolar gene expression that follow RPA KD were accompanied by changes in nucleolar morphology, specifically reductions in size. Together, our results reveal novel functions for the RPA complex in maintaining nucleolar homeostasis.

Results

SETX depletion promotes nucleolar RPA localization

As indicated above, a number of proteins have been implicated in the cellular response to R loops, and SETX and RPA are two significant ones. Given that the proteins share several common properties, such as functioning in RNAP II transcription, associating with nucleolin, and functioning in R-loop resolution, in part by recruiting other factors (Richard et al. 2013; Nguyen et al. 2017), we wondered whether their functions might be partly redundant or complementary. To address this possibility, we initially asked how depletion or loss of SETX might affect RPA localization and/or its function in the nucleus. We first performed immunofluorescence (IF) assays to examine RPA subcellular localization in HeLa cells treated with either of two SETX siRNAs (siSETX and siSETX2) or a negative control siRNA (NC). SETX knockdown (KD) efficiencies, determined by Western blot (WB) are shown in Supplemental Figure S1A. As expected (e.g., Liu et al. 2017), RPA (specifically, RPA70) localized relatively uniformly throughout the nucleus/nucleolus in the presence of the control siRNA. Treatment with either SETX siRNA, however, resulted in striking RPA70 nucleolar localization, colocalizing with the nucleolar marker fibrillarin (Fig. 1A; zoomed images with more cells are shown in Supplemental Fig. S1B). Quantification of the images revealed that RPA70 in SETX KD cells showed an increased nucleolar to nuclear ratio relative to the NC group (Supplemental Fig. S1C). This relocalization did not reflect changes in RPA protein amounts, as WB revealed that levels of RPA70 and RPA32 were unaffected by SETX KD (Supplemental Fig. S1A).

The roles of RPA and SETX in R-loop resolution and the fact that R loops are abundant at rDNA led us to hypothesize that excess R-loop formation underlies RPA

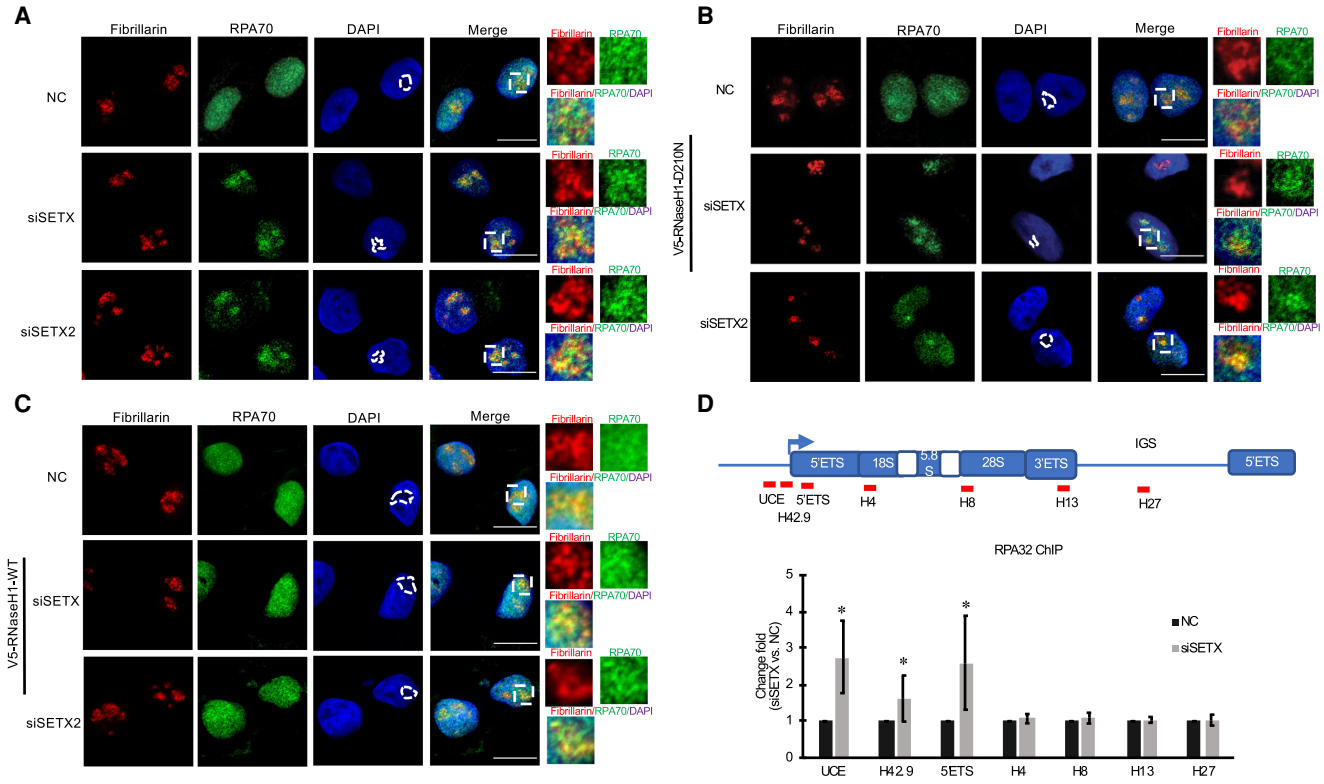

Figure 1. SETX depletion leads to R-loop-dependent nucleolar RPA localization. Representative images of nucleolar RPA70 localization measured by its colocalization with fibrillarin. Cells were transfected with NC (negative control) siRNA or siRNAs targeting SETX (siSETX or siSETX2) at 20 nM for 72 h. Cells were stained for fibrillarin (red) or RPA70 (green), and with DAPI (blue). Scale bar, 15 µm. SETX KD was performed in HeLa (*A*), V5-RNaseH1 D210N (*B*), and V5-RNaseH1 WT (*C*) cells. The outlined areas in the merged images (cropped from panels) are shown at the *right*. (*D*) ChIP-qPCR experiments along the rDNA locus (illustrated in schematic at the *top*; red bars indicate positions of primers) to determine RPA32 occupancy in SETX KD and control HeLa cells. Probes were designed to detect upstream core element (UCE), promoter regions (H42.9 and 5′ETS), gene body (H4 and H8), and the intergenic spacer (H13 and H27). Significance was analyzed by a Student's *t*-test. (*) $P < 0.05$. $n = 3$.

nucleolar localization following SETX depletion. To investigate this, we constructed and used two HeLa cell lines that express RNaseH1 derivatives, V5-RNaseH1-WT and V5-RNaseH1-D210N (Chen et al. 2017), to visualize RPA70 localization following SETX KD. V5-RNaseH1-D210N is a mutant V5 epitope-tagged RNaseH1 derivative that binds to but does not cleave RNA:DNA hybrids, while elevated levels of the WT derivative degrade R loops. IF indicated that both proteins localized to the nucleus as expected (Supplemental Fig. S2A [expression levels and SETX KD efficiencies were verified by WB], B,C; Chen et al. 2017). In controls without SETX KD (NC), RPA70 was detected throughout the nucleus in both V5-RNaseH1-WT and V5-RNaseH1-D210N cells (Fig. 1B,C), similar to what we observed in HeLa cells (see Fig. 1A). Following SETX depletion in the V5-RNaseH1-D210N cells (siSETX and siSETX2), RPA70 accumulated in nucleoli, colocalizing in foci with fibrillarin (Fig. 1B), again as observed with HeLa cells. Strikingly, however, RPA70 nucleolar localization, and colocalization in foci with fibrillarin, were greatly reduced after SETX KD in the V5-RNaseH1-WT cells compared with V5-RNaseH1-D210N cells, and RPA70 localization was very similar to that observed in control (NC) cells (Fig. 1C). Together, these results show that depletion of SETX results in accumulation of RPA in nucleolar foci, and that this localization appears to depend on the presence of R loops on rDNA.

To confirm that the nucleolar RPA was indeed associated with rDNA, we used chromatin immunoprecipitation (ChIP) to analyze the association of RPA with rDNA. We performed RPA32 ChIP assays with HeLa cells treated with control or SETX siRNAs. Interestingly, we observed a significant increase in RPA32 at rDNA promoter regions (UCE, H42.9, and 5′ETS) in SETX KD compared with control cells, but not in the rDNA gene body (H4 and H8), 3′ETS (H13), or intergenic spacer (IGS; H27) (Fig. 1D). If this chromatin association indeed reflects binding to R loops, then it was initially surprising to detect ChIP signals upstream of the rRNA transcription start site. However, as described below, a likely possibility is that this reflects R-loop formation involving pRNAs transcribed from upstream SPs and/or antisense *PAPAS* transcripts. In any event, our data show that RPA is recruited to rDNA promoter regions upon loss of SETX, correlating with its accumulation in the nucleolus.

RPA colocalizes with nucleolar R loops in AOA2 patient fibroblasts

The above data showed that loss of SETX can drive R-loop-dependent RPA nucleolar localization. Given that AOA2 is characterized by SETX loss of function, we next asked whether RPA localizes to nucleoli in AOA2 patient cells, and whether this reflects elevated levels of R loops. We obtained skin biopsies from a family of three, two members of which had been diagnosed with AOA2 (Mut-1 and Mut-2), while a sibling carried a missense mutation but was without disease symptoms (WT) (Richard et al. 2021). To detect R loops, we used the S9.6 antibody, which recognizes RNA:DNA hybrids in R-loop structures. We speculated that *SETX* mutations interfering with R-loop resolution might bring about RPA70 association with R loops in the mutant but not WT fibroblasts. As expected, RPA70 IF revealed accumulation of the protein throughout the nucleus in WT and mutant cells (Fig. 2A). Strikingly, though, in the Mut-1 and Mut-2 fibroblasts, RPA70 showed strong punctate staining, and costaining with S9.6 revealed that RPA70 indeed colocalized with R loops in these foci (Fig. 2A); the significant cytoplasmic S9.6 staining has been observed previously (García-Rubio et al. 2015; Shen et al. 2017; Grunseich et al. 2018) and may reflect mitochondrial R loops. To confirm that the RPA70- and R-loop-containing foci were nucleoli, we costained cells for RPA70 and fibrillarin as above, which indeed revealed colocalization (Fig. 2B). These findings were confirmed by plot profile analysis (Fig. 2C). The colocalization of RPA, fibrillarin, and R loops suggests that RPA is present at R loops formed on nucleolar rDNA in AOA2 patient fibroblasts.

RPA relocalization to the nucleolus is also induced by Top1 inhibition

The above data showed that loss of SETX leads to accumulation of R loops and, as a result, of RPA in the nucleolus. We next investigated whether other treatments that enhance R loops on rDNA lead to RPA nucleolar accumulation. To this end, we treated HeLa cells with CPT, which transiently induces nucleolar R-loop formation by stabilizing Top1–DNA cleavage complexes (Marinello et al. 2013; Shen et al. 2017), and performed IF to detect RPA70 and RNAP I in control and treated cells. (We visualized RPA194 as opposed to fibrillarin both as a second nucleolar marker and also to determine more directly

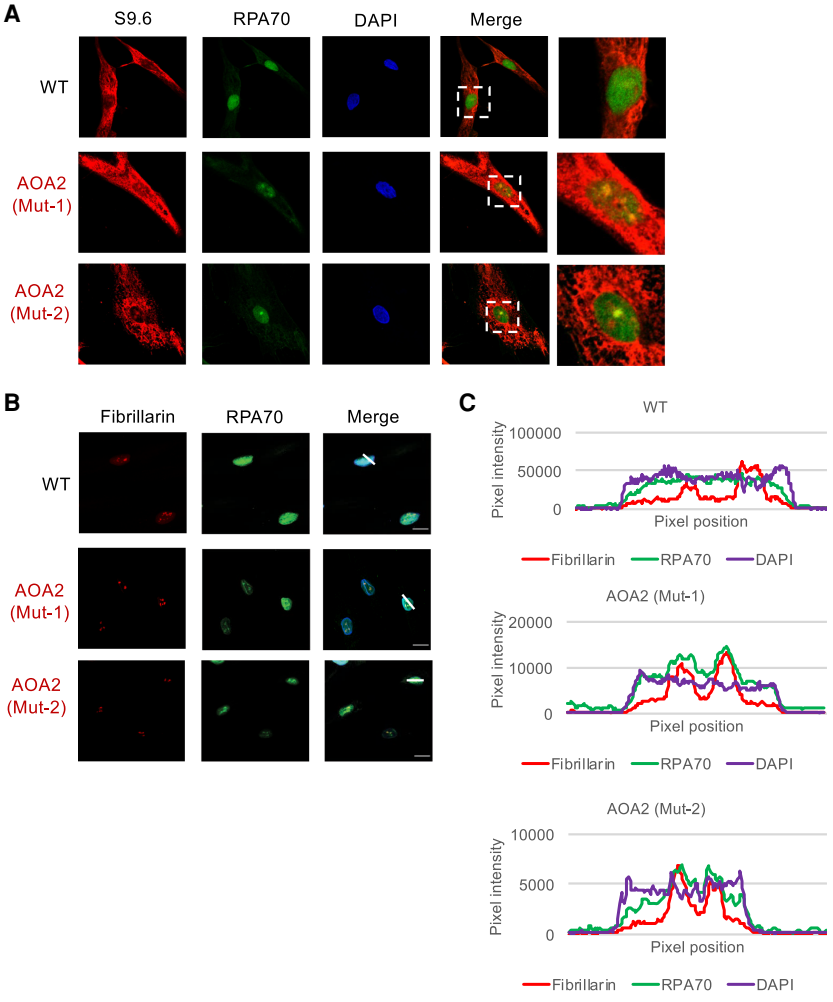

Figure 2. Nucleolar RPA70 colocalizes with R loops in AOA2 patient fibroblast cells. AOA2 patient fibroblasts (Mut-1 and Mut-2) and normal fibroblasts (WT) were stained with appropriate antibodies for R loops (S9.6, red) and RPA70 (green) (*A*), and fibrillarin (red) and RPA70 (green) (*B*). (*A*) DAPI staining and merged images are shown as indicated. The outlined areas are shown enlarged at the *right*. Scale bar, 15 µm. (*C*) Analysis of colocalization of RPA70 and fibrillarin in AOA2 fibroblast cells. Fluorescence intensity profiles of RPA70 (green lines), fibrillarin (red), and DAPI (blue) show the distribution of fluorescence across the lines in merge images in *B* (*X*-axis). Fluorescence intensities are indicated on the *Y*-axis. Green and red coincident peaks indicate colocalization.

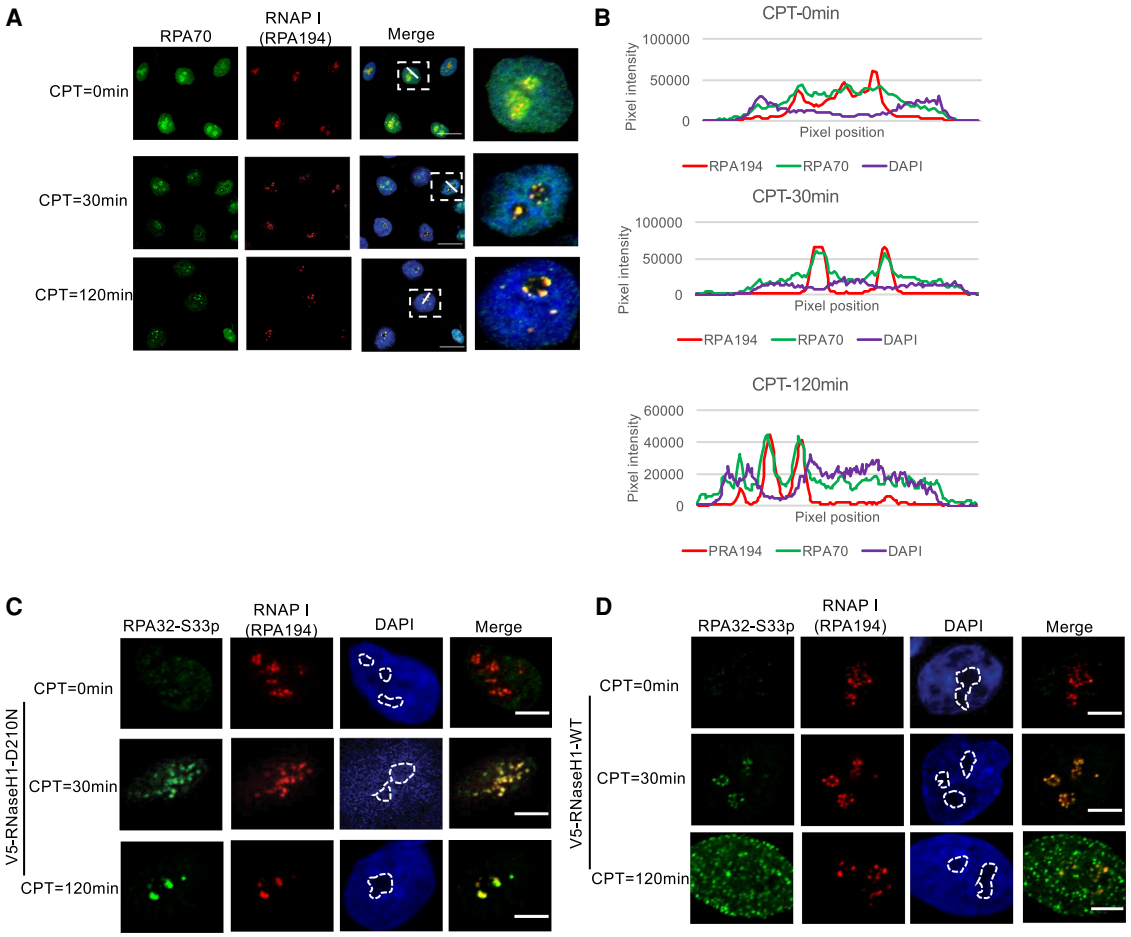

Figure 3. RPA translocation into the nucleolus and accumulation at rDNA regions following CPT treatment is R-loop-dependent. (*A*) Representative confocal immunofluorescence images of HeLa cells treated with 25 µM CPT for 0, 30, or 120 min. Cells were stained with appropriate antibodies for RNAP I subunit RPA194 (red) and RPA70 (green) and with DAPI (blue). The outlined areas are shown enlarged at the *right*. Scale bar, 15 µm. (*B*) Analysis of colocalization of RPA70 and RPA194 with or without CPT treatment. Fluorescence intensity profiles of RPA70 and RPA194 show the distribution of fluorescence across the lines in merged images in *A* (*X*-axis). Fluorescence intensities are plotted along the *Y*-axis and the green and red coincident peaks indicate colocalization. IF of RPA32 Ser33 phosphorylation (RPA32-S33p) following CPT treatment for the indicated times in V5-RNasseH1-D210N cells (*C*) and V5-RNaseH1-WT cells (*D*). (Red) RPA194, (green) RPA32-S33p, (blue) DAPI. Nucleoli are circled. Scale bar, 5 µm.

whether RPA colocalizes to sites of rDNA transcription.) As expected, RPA70 was distributed throughout the nucleus with a significant signal in the nucleolus in the control cells (NT), but colocalization with RNAP I was minimal (Fig. 3A [plot profile analysis in B]). However, we observed significant RPA-RNAP I colocalization after 30-min exposure to 25 µM CPT, and these complexes appeared to comigrate to the perinucleolar region after 120 min of CPT treatment (Fig. 3A,B). To confirm that CPT indeed induced DNA damage, we examined γH2AX levels, a marker of DNA double-strand breaks (DSBs), by WB, and observed a significant increase of γH2AX after both 30 and 120 min of CPT treatment (Supplemental Fig. S3A). WB also revealed that RPA70 and RPA32 levels were not changed by CPT treatment (Supplemental Fig. S3A). However, we observed an increase in phosphorylated RPA32 (RPA32-S33p) (Toledo et al. 2013) following CPT treatment for 30 or 120 min (Supplemental Fig. S3A). This is notable because RPA32-S33p has been shown to be present in RPA complexes involved in R-loop resolution (Nguyen et al. 2017; Promonet et al. 2020). Interestingly, we also observed that SETX levels were decreased by CPT treatment (Supplemental Fig. S3A), perhaps contributing to the increase in R loops. Together, these data indicate that RPA relocalizes to the nucleolus in response to CPT-induced genotoxic stress, similar to its behavior in the absence of SETX.

To extend these results, we investigated whether CPT-induced colocalization of RPA with RNAP I in the nucleolus was in fact R-loop-dependent. To this end, we used the V5-RNaseH1-WT and V5-RNaseH1-D210N RNaseH1-expressing cells described above, and stained the cells in this case with an antibody directed against RPA32-S33p. In the V5-RNaseH1-D210N cells, we observed that RPA32-S33p was not localized significantly to the nucleolus in the absence of CPT treatment

(CPT = 0 min), consistent with previous findings (Promonet et al. 2020). With CPT treatment, RPA32-S33p localization was very similar to what we observed with RPA70 in HeLa cells: Colocalization with RNAP I was readily apparent after 30-min CPT treatment, and interestingly, the presumptive RPA/RNAP I complexes appeared again to relocalize to the perinucleolar region after 120-min CPT treatment (Fig. 3C). In the V5-RNaseH1-WT cells, with CPT treatment for 30 min, RPA/RNAP I complexes were detected at the perinucleolar region, patterns that were similar to those observed in V5-RNaseH1-D210N cells after 120-min CPT. Strikingly, after 120 min, RPA32-S33p, but not RNAP I, nucleolar staining was greatly reduced, and localization to the nucleolar periphery was minimal (Fig. 3D; additional cells shown in Supplemental Fig. S3B,C). These results provide strong evidence that R-loop formation is required for RPA colocalization with RNAP I in the nucleolus following genotoxic stress.

The above data indicate that the Top1 inhibitor CPT induces RPA relocalization in the nucleolus in an R-loop-dependent manner. To determine whether loss of Top1 has a similar effect, we knocked down Top1 in HeLa cells with an siRNA for 72 h, and then analyzed RPA70 localization by IF. Indeed, we observed intense nucleolar RPA70 foci upon Top1 KD (siTop1) compared with the negative control siRNA (NC) (Supplemental Fig. S3D [plot profile analysis in E]). Signal intensities were quantified, which revealed that the nucleolar to nuclear RPA70 ratio was significantly increased after Top1 KD (Supplemental Fig. S3F). WB showing Top1 and RPA70 levels following Top1 KD is shown in Supplemental Figure S3G. Given that RPA70 levels were unchanged, the data together indicate an increase of RPA in the nucleolus following Top1 KD.

Loss of RPA results in accumulation of R loops and R-loop-induced DSBs

The experiments described above have shown that RPA localizes to sites of excess R-loop formation, notably in the nucleolus. This likely reflects a role in resolution of these R loops (Nguyen et al. 2017), but the above experiments did not provide direct evidence for this. In addition, it is well known that loss of RPA induces replication and DNA repair defects (Hass et al. 2012; Toledo et al. 2017), but whether either of these might result at least in part as a consequence of R-loop formation is not known. To investigate whether RPA prevents R-loop accumulation and whether its function in maintaining genome stability is R-loop-dependent, we first performed IF with the S9.6 antibody to detect R loops in RPA KD HeLa cells. For this, we used siRNAs targeting RPA70 and RPA32 separately (siRPA70 and siRPA32). RPA70 and RPA32 siRNA KD efficiencies were determined by WB (Supplemental Fig. S4A). Strikingly, we found that loss of either RPA32 or RPA70 resulted in significant increases in nucleolar S9.6 staining relative to cells treated with a control siRNA (NC) (Fig. 4A [quantitation shown in B]). To ensure the specificity of the S9.6 signals, GFP-RNaseH1 was expressed in control KD cells. This S9.6 staining was essentially eliminated in cells expressing GFP-RNaseH1 (Fig. 4C). Additional examples are shown in Supplemental Figure S4B (top panel); cells without expression GFP-RNaseH1 are also shown (bottom panel). RPA70 and RPA32 siRNA KD efficiencies were determined by WB (Supplemental Fig. S4C [note that here and in A depletion of one RPA subunit resulted in codepletion of the other, as has been observed previously]; Wu et al. 2005).

We next investigated whether the function of RPA in maintaining genomic stability reflects its function in R-loop resolution. Previous studies have shown that depletion of RPA subunits induces DSBs, and it is also well known that accumulation of R loops leads to DSBs (Li and Manley 2005; Bhatia et al. 2014; Hatchi et al. 2015). To determine whether R loops play a role in the DSBs induced by RPA loss, we first measured accumulation of γH2AX by IF and found that RPA32 KD as expected increased accumulation of γH2AX foci; i.e., DSBs (Fig. 5A, left panels [quantitation in B]). Importantly, the increased γH2AX signal was eliminated in cells expressing GFP-RNaseH1 (Fig. 5A, right panels [quantitation in B]). RPA70 and RPA32 siRNA KD efficiencies were determined by WB with or without GFP-RNaseH1 expression (Supplemental Fig. S4A,C). It is noteworthy that background γH2AX levels were not reduced by GFP-RNaseH1 expression, suggesting that whatever DNA damage this signifies does not reflect R loops. To confirm these results, we used the V5-RNaseH1-WT and V5-RNaseH1-D210N cells and two different siRNAs to target RPA32 (siRPA32 and siRPA32-2) and measured γH2AX levels by WB. We found that both siRNAs increased γH2AX levels twofold to threefold compared with negative controls (NC) in the D210N cells, while γH2AX levels were unchanged by RPA32 KD in the WT RNaseH1 cells (Fig. 5C [quantitation in D]). Thus, our data together strongly suggest that the role of RPA in preventing DSBs reflects at least in part its function in resolving R loops, and supports the view that its recruitment to sites of R-loop formation in nucleoli following replication stress is to counteract R-loop-dependent DNA damage.

RPA depletion reduces rRNA transcription by an R-loop-dependent mechanism

R loops by definition occur during transcription. We therefore next set out to determine whether RPA function in resolving R loops in the nucleolus affects rRNA transcription. To this end, we used siRNAs targeting RPA32 in the V5-RNaseH1-WT and V5-RNaseH1-D210N cells and as a measurement of transcription determined 47S pre-rRNA levels by RT-qPCR (probes used are indicated in diagrams above figures; Zhao et al. 2016a; Shen et al. 2017; Zhao et al. 2018). We found that RPA32 depletion led to an ~30%–40% decrease in 47S pre-rRNA levels in the mutant RNaseH1 cells (Fig. 6A). Strikingly, though, 47S transcript levels were unaffected in the WT RNaseH1 cells (Fig. 6A). To confirm these results, we determined the effects of RPA KD on rRNA transcription by measuring 5-fluorouridine (FUrd) incorporation by IF (Supplemental Fig. S5). The results reveal that RPA32 KD

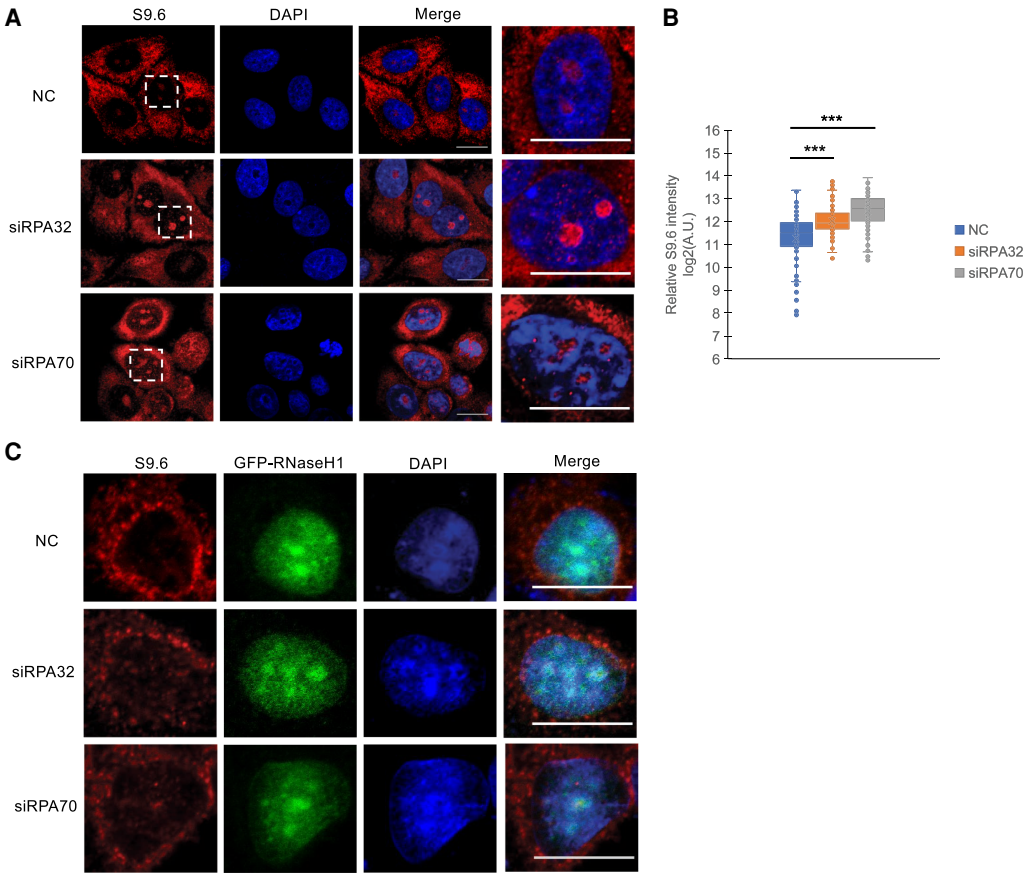

Figure 4. Loss of RPA increases R loop accumulation in nucleoli. (*A*) HeLa cells were transfected with a control siRNA (NC), siRPA32, or siRPA70 for 72 h. Cells were stained for R loops using the S9.6 antibody (red) and with DAPI (blue). Scale bar, 15 µm. The area in dashed boxes is shown enlarged at the *right*. Scale bar, 5 µm. (*B*) Box plot quantification of S9.6 foci intensity per cell as shown in *A*. Significance was analyzed by a Student's *t*-test. (***) $P < 0.001$; cell number: $n = 150$. (A.U.) Arbitrary unit. (*C*) HeLa cells expressing GFP-RNaseH1 were transfected with an siRNA control (NC), siRPA32, or siRPA70 for 72 h. Cells were stained for R loops using the S9.6 antibody (red) or with DAPI (blue). Scale bar, 5 µm.

inhibited rRNA transcription in V5-RNAseH1-D210N-expressing cells (S5A) but not in cells expressing V5-RNAseH1-WT (S5B). These findings suggest that RPA functions in rRNA transcription, likely by a mechanism that involves resolving R loops that otherwise exert a repressive effect on RNAP I transcription.

The above experiments provide evidence that loss of RPA negatively impacts rRNA transcription in an R-loop-dependent manner. To confirm that this reflects accumulation of R loops on rDNA, we carried out ChIP analysis with V5 antibodies using the V5-RNaseH1-D210N cells following RPA KD. As mentioned above, the D210N derivative binds R loops but fails to resolve them, and can thus be used to detect R loops along the genome (Chen et al. 2017; Tan-Wong et al. 2019). We observed accumulation of R loops at rDNA promoter regions, most notably over the upstream UCE (see below), and more modest increases along the rDNA gene body after RPA32 KD (siRPA32 and siRPA32-2) compared with a control KD (NC) (Fig. 6C). To confirm the R-loop signals we observed were due to V5-D210N RNaseH1 binding to R loops, we performed V5 ChIP using HeLa cells expressing another V5 RNaseH1 mutant derivative, WKKD, which fails to recognize R loops (Chen et al. 2017). With these cells, we did not detect R-loop accumulation at rDNA promoter regions following RPA32 KD (Supplemental Fig. S6A).

We also examined whether loss of RPA affects RNAP I occupancy along rDNA. To this end, we again used ChIP with the V5-RNaseH1-D210N cells, in this case with an anti-RPA194 antibody, to detect RNAP I on rDNA. Interestingly, we observed an increase in RNAP I on rDNA promoter regions following RPA32 KD that was similar to the pattern detected with the V5 antibody, notably with the strongest signal over the UCE (Fig. 6C). Importantly, elevated RNAP I levels were not observed in the V5-RNaseH1-WT-expressing cells after RPA32 KD (Supplemental Fig. S6B). Therefore, our results together show that loss of RPA32 increased R-loop formation/stability and RNAP I occupancy on rDNA.

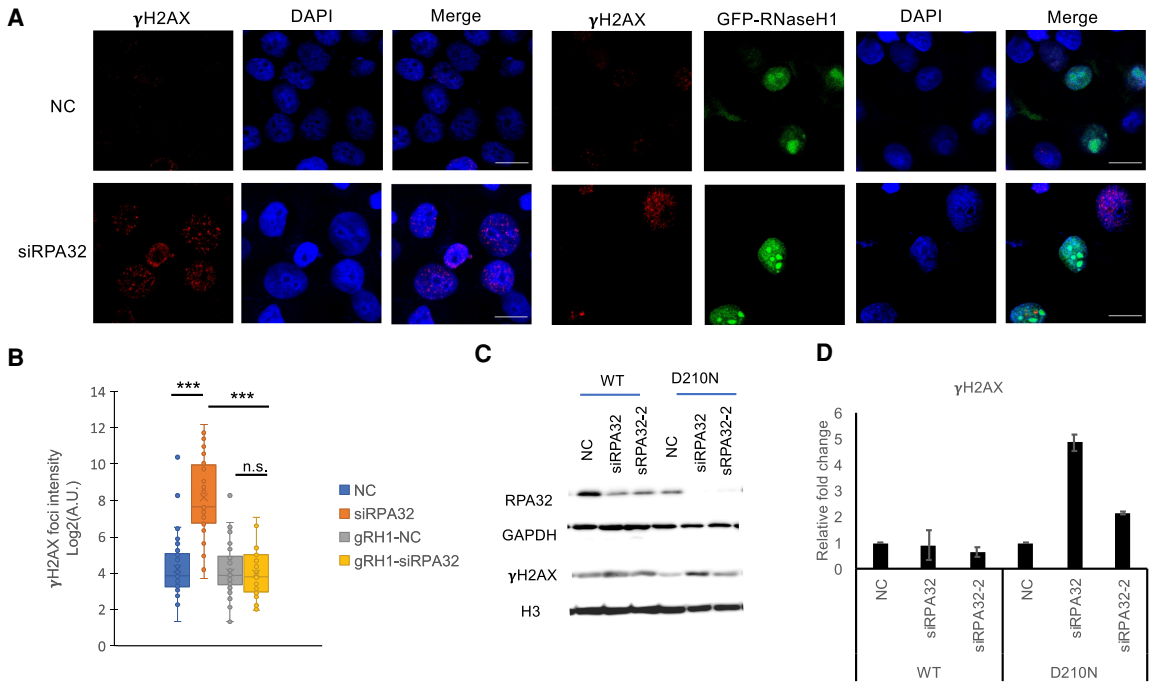

Figure 5. RPA depletion results in R-loop-dependent genomic instability. (*A*) HeLa cells were transfected with an siRNA control (NC) or two different siRNAs targeting RPA32 (siRPA32 and siRPA32-2), with or without expression of GFP-RNaseH1 for 24 h, 48 h after siRNA transfection. Cells were analyzed by IF using γH2AX antibodies (red), GFP (green), and DAPI (blue). (*B*) Box plot quantification of γH2AX focus intensity per cell as shown in *A*. Significance was analyzed by a Student's *t*-test. (***) $P < 0.001$, (n.s.) no significance. At least 40 cells were counted under each condition. (*C*) γH2AX and RPA32 levels were analyzed by WB after siRPA32 KD in V5-RNaseH1-WT and V5-RNaseH1-D210N cells. GAPDH and histone H3 levels are also shown. (*D*) Quantitation of γH2AX levels. Relative γH2AX fold changes following RPA32 KD as shown in *C* were normalized to H3 levels and compared with NC. SE shown. $n = 3$.

R loops induced by RPA KD increase PAPAS *and pRNA transcription*

We next wished to investigate how the increase in R loops detected after RPA KD might contribute to reductions in rRNA transcription. Elevated levels of antisense *PAPAS* transcription, as mentioned above, can repress rRNA transcription (Zhao et al. 2018; Xiao et al. 2020). We therefore examined whether RPA KD increases *PAPAS* expression. To examine this, we performed strand-specific RT-qPCR using primers that cover distinct regions of the rDNA repeats (Fig. 6D, primer positions are shown in schematic). Strand specificity was ensured by reverse transcription with primers linked to a T7 promoter sequence, followed by PCR amplification of the cDNA with an rDNA-specific primer and the T7 promoter primer (Zhao et al. 2016b). Notably, we observed a significant increase of *PAPAS* RNA after RPA32 KD in V5-RNaseH1-D210N cells, but importantly, this increase was not observed in the V5-RNaseH1-WT cells. We used a second set of primers (H0) to confirm these results, and again observed increased *PAPAS* levels following RPA32 KD (Supplemental Fig. S7A). We also knocked down RPA70 and observed a very similar increase in *PAPAS* levels in the V5-D210N but not V5-WT RNAseH1-expressing cells (Supplemental Fig. S7B). We next examined pRNA levels following RPA KD. As mentioned above, pRNAs, transcribed in the sense direction from intergenic SPs, can also contribute to silencing of rRNA transcription (Schmitz et al. 2010). We therefore performed strand-specific RT-qPCR to measure pRNA levels (Fig. 6E). We indeed observed a significant increase in pRNA levels partially extending over the UCE after RPA32 KD in V5-RNaseH1-D210N cells. Significantly, though, this increase was not observed in the V5-RNaseH1-WT cells. We also used a second set of primers to confirm these results, and observed similar increased pRNA levels following RPA32 KD (Supplemental Fig. S7C). 47S, *PAPAS*, and pRNA levels are shown merged in the same diagram to facilitate comparison (Supplemental Fig. S7D). These results together provide evidence that RPA plays a role in suppressing *PAPAS* and pRNA transcription by reducing R-loop accumulation.

RPA32-deficient cells have a structurally disorganized nucleolus

We next examined whether the effects on R-loop formation and transcription in the nucleolus observed following RPA depletion might affect nucleolar organization or structure. RNAP I inhibition has been found to activate a nucleolar stress response that results in reorganization of nucleolar components (Bywater et al. 2012) and inhibition of rRNA transcription coupled with nucleolar

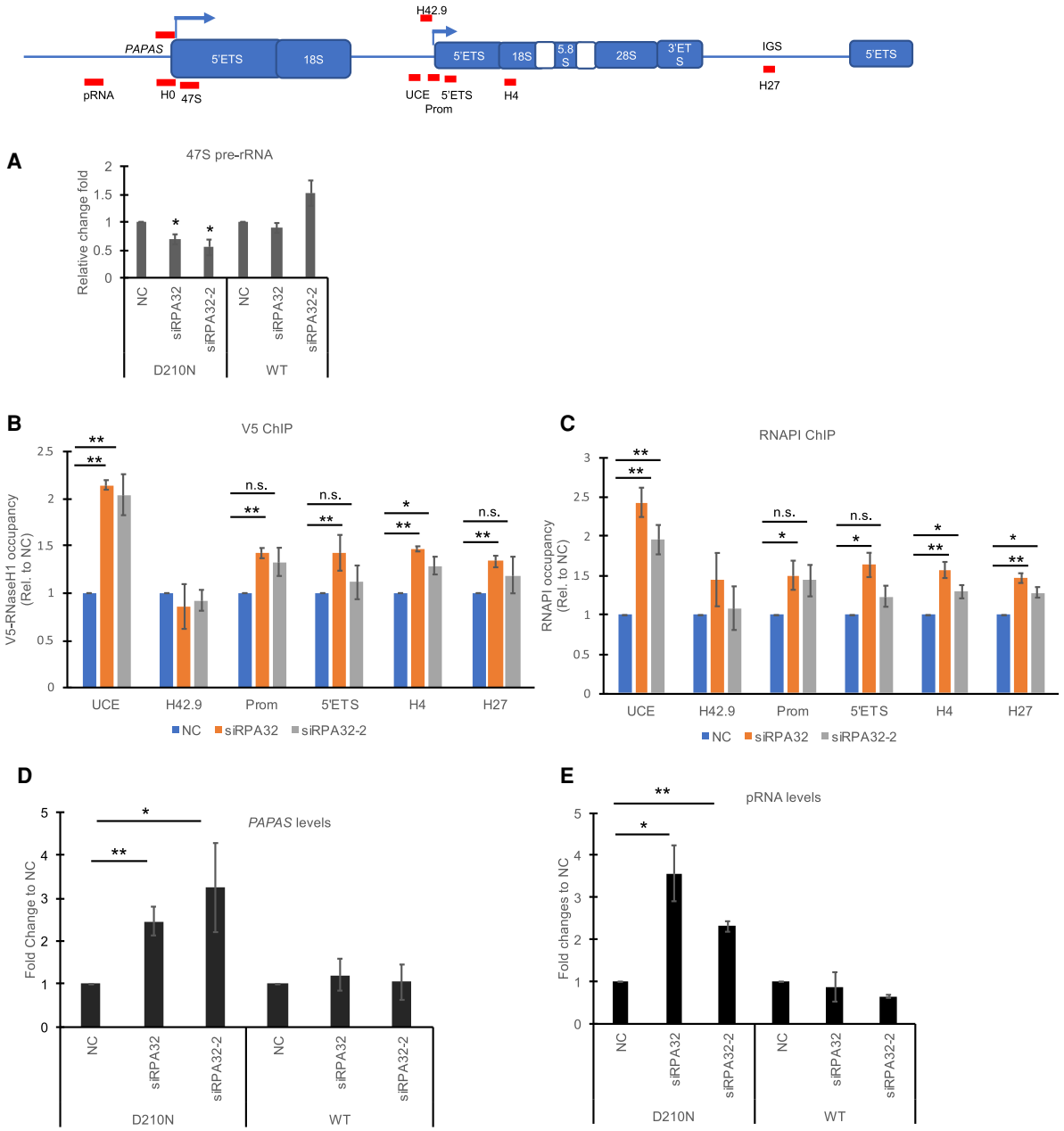

Figure 6. Loss of RPA32 inhibits rRNA transcription and increases *PAPAS* and pRNA expression in an R-loop-dependent manner. (*A*) RT-qPCR quantification of 47S pre-rRNA levels after siRPA32 KD in V5-RNaseH1-D210N or V5-RNaseH1-WTcells. SE shown. $n = 3$. Statistical analysis was performed using a Student's *t*-test. (*) $P < 0.05$. Schematics of rRNA locus are shown and positions of probes are indicated by red bars. (*B*) R-loop distribution along rDNA locus was determined using V5 ChIP in V5-RNaseH1-D210N cells, with probes designed to recognize the UCE, H42.9, 5′ETS, H4, and H27 regions. (*C*) RNAP I occupancy along the rDNA; RNAP I was immunoprecipitated by RPA194 antibody. SE shown. $n = 3$. Statistical analysis was performed using a Student's *t*-test. (*) $P < 0.05$, (**) $P < 0.01$, (n.s) no significance. RT-qPCR quantification of antisense rRNA *PAPAS* (*D*) or pRNA (*E*) levels by strand-specific qPCR. Positions of probes are indicated by red bars in the schematic *above*. Cells were transfected with two different siRNAs targeting RPA32 (siRPA32 and siRPA32-2). Values were normalized to GAPDH in V5-RNaseH1-WT and V5-RNaseH1-D210N cells. Data are presented as mean and SE ($n = 3$). (*) $P < 0.05$, (**) $P < 0.01$.

structural changes (Sokka et al. 2015). To investigate whether loss of RPA, and the resulting effects on nucleolar transcription, affects nucleolar morphology, we performed IF first with V5-RNaseH1-D210N cells following RPA32 KD using anti-RPA194 antibodies (Fig. 7A,B). As expected, IF of cells treated with a control siRNA revealed one to three large and spherical intranuclear masses corresponding to nucleoli (NC group). In contrast, the nucleolar masses appeared distorted and fragmented into several smaller masses of reduced size in the RPA32 KD cells

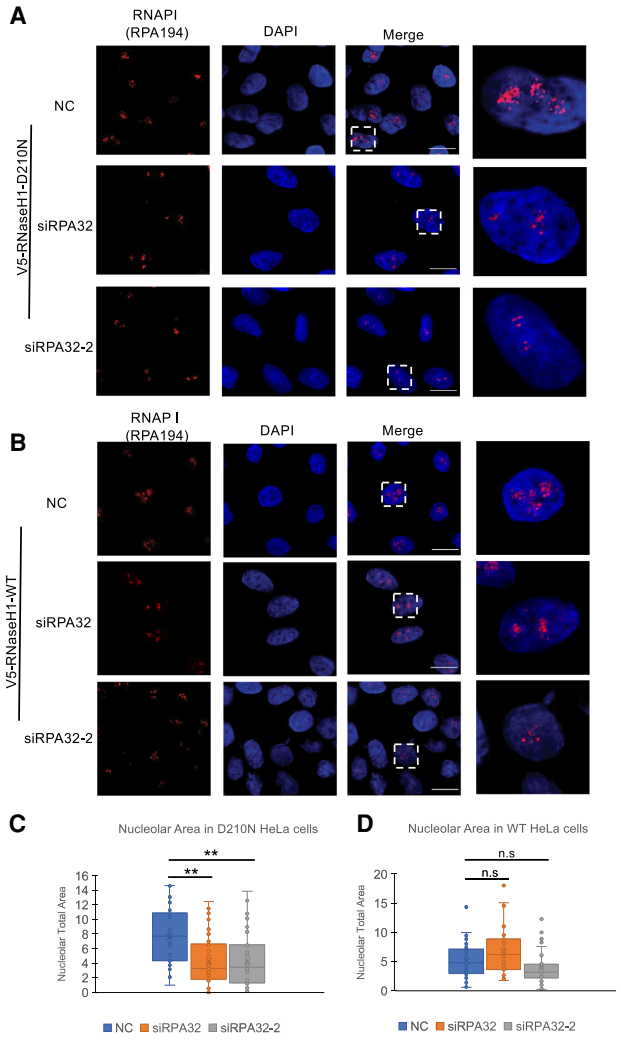

Figure 7. RPA32 KD promotes R-loop-dependent nucleolar disorganization. Immunolocalization of RNAP I and DAPI staining in RPA32-depleted cells. V5- RNaseH1-D210N (*A*) and V5-RNaseH1-WT (*B*) cells were transfected with a control (NC) or one of two different siRNAs targeting RPA32 (siRPA32 and siRPA32-2). Cells were stained for RNAP I (RPA194, red) or with DAPI (blue). Areas highlighted in the "Merge" fields are shown enlarged at the *right*. Scale bars, 15 µm. Total nucleolar areas in the V5- RNaseH1-D210N (*C*) and V5-RNaseH1-WT cells (*D*) were quantified and are presented as box plots as described in the Materials and Methods. More than 50 cells from three independent repeats were quantified, (**) $P < 0.01$, (n.s) no significance.

(siRPA32 and siRPA32-2). Quantification of the images revealed that the median nucleolar size, or area, was indeed significantly reduced, by ~twofold, following RPA32 depletion (Fig. 7C). Given that we observed that R loops affect rDNA transcription, we wondered whether R loops also drive the nucleolar morphological changes that we detected following RPA32 depletion. To test this possibility, we knocked down RPA32 in V5-RNaseH1-WT cells and performed the same IF experiments as above. Strikingly, IF revealed that these cells exhibited normal nucleolar morphology, and quantitation indicated nucleolar size was not significantly changed by RPA32 KD (Fig. 7B,D). Thus, these results suggest that RPA may act as a natural guardian of nucleolar structure and function.

Discussion

Cotranscriptional R loops play important, well-known roles in several cellular processes, but perhaps more frequently they can be highly deleterious when they form unnaturally. It is thus not surprising that multiple protein factors have been implicated in preventing inappropriate R-loop formation and in resolving these structures when they do form. In this study, we set out initially to investigate whether two such factors, SETX and RPA, might functionally interact in some way, and our results led to our discovery of an unexpected role for RPA in modulating R-loop formation in the nucleolus and, as a result, in the maintenance of nucleolar homeostasis. Below we discuss this novel nucleolar role for RPA, how this impacts nucleolar transcription by RNAP II as well as RNAP I, and how this affects nucleolar structure.

Maintenance of nucleolar homeostasis is crucial for cells to respond to stress, and is typically linked to inhibition of rRNA transcription and/or changes in nucleolar morphology and composition. In mammalian cells, an inappropriate stress response leads to either cell cycle arrest or apoptosis, depending on the cell's ability to recover. It is known that RNAP I-mediated transcription is significantly disrupted in response to rDNA-specific DNA damage, as well as DNA damage induced outside nucleoli (Kruhlak et al. 2007; Harding et al. 2015; Larsen and Stucki 2016). CPT treatment or loss of Top1, which causes DNA damage, was shown to slow or impede RNAP I elongation significantly, and this is coupled with increased formation of R loops on rDNA (Christensen et al. 2004; Koster et al. 2007; Aguilera and Gómez-González 2008; El Hage et al. 2010; Manzo et al. 2018). Furthermore, Sen1 (in yeast) and RNaseH1 are known to function in suppression of R loops in the nucleolus (Drolet et al. 1995; El Hage et al. 2010; Skourti-Stathaki et al. 2011; Chan et al. 2014; Shen et al. 2017; Manzo et al. 2018). However, these studies failed to link increased nucleolar R-loop formation with defects in nucleolar structure and rRNA gene transcription. Therefore, we undertook to identify additional factors that might function in nucleolar R-loop metabolism and in regulating nucleolar function. In this study, we showed that RPA also plays an important role in combatting nucleolar R loops. As we discuss, this role becomes especially prominent when SETX levels are reduced, either experimentally by depletion, by mutation in disease, or perhaps by DNA damage.

It was striking that reduced SETX levels in cells drive elevated RPA nucleolar localization and increases its occupancy at and around rDNA promoters. SETX functions in diverse ways to modulate R loops and, as a result, transcription. For example, SETX plays a role in the R-loop-dependent DNA damage response (Skourti-Stathaki et al. 2011; Yuce and West 2013; Hatchi et al. 2015; Cohen

et al. 2018), and colocalizes with several proteins, including Top1, 53BP1, and γH2AX, and the nuclear exosome at transcription–replication stress foci when transcription and replication machineries collide (Suraweera et al. 2007; Becherel et al. 2013; Richard et al. 2013; Yuce and West 2013). Our results showing that, following SETX depletion, RPA colocalizes with R loops that accumulate at rDNA promoter regions (e.g., the UCE, promoter, and 5′ ETS) (see model in Fig. 8.), which have been reported as sites of R-loop formation (Manzo et al. 2018; Abraham et al. 2020), are consistent with previous findings in yeast that loss of Sen1 significantly increases R loops in rDNA regions (Chan et al. 2014; El Hage et al. 2014). These stabilized R loops generate excess stretches of ssDNA that generate binding sites for RPA, which in turn recruits and activates RNaseH1, facilitating R-loop resolution (Nguyen et al. 2017). Additionally, increased RPA occupancy was also observed at rDNA promoters under hypo-osmotic conditions, and this appeared coupled with stabilized R loops, which results in ATR pathway activation (Velichko et al. 2019).

Increased RPA accumulation in the nucleolus likely impacts its function in maintaining genome stability throughout the nucleus. RPA is a well-known sensor of DNA replication stress and DNA damage, for example, serving as a platform to recruit the ATR kinase and other proteins (Zou and Elledge 2003; Li and Zou 2005; Toledo et al. 2013; Maréchal and Zou 2015). Our finding that RPA accumulates in nucleoli in response to certain stresses, while total levels are unchanged, indicates a corresponding depletion of RPA in the nucleus under these conditions, and it is possible that this contributes to elevated levels of R loops in the nucleus. Insufficient RPA levels can also induce DNA damage and replication catastrophe due to unresolved replication fork stalling and inhibition of checkpoint progression (Toledo et al. 2013, 2017). Our results following RPA KD are both consistent with these findings, as we observed a significant increase in γH2AX in the nucleus in the absence of RPA, and also extend them by implicating R loops in this response, as γH2AX accumulation was eliminated by RNaseH1 overexpression. Notably, a similar phenotype has been reported under conditions of hypo-osmotic stress: RPA (and other DNA repair factors) accumulated in nucleoli where R loops were detected, and cells exhibited increased γH2AX (Velichko et al. 2019). Our results extend these findings in several ways, notably by showing that RPA nucleolar localization in response to stress actually requires the presence of R loops. These findings define a novel function for RPA in maintaining genomic stability that is independent of its role as a DNA replication or repair factor, which is to respond to excess R loops and prevent resultant DNA damage.

Our studies revealed a significant increase of R loops in and around rDNA promoters following RPA depletion. Notably, the GC content in the UCE region is ~70% (Wehner et al. 2014), conducive to R-loop formation. This is consistent with our data demonstrating elevated R-loop formation at the UCE following RPA KD, coupled with increased RNAP I occupancy and decreased pre-rRNA levels. However, R loops at RNAP II promoters, which are often linked to unmethylated CpG islands, prevent DNA methylation and thus facilitate target gene transcription (Ginno et al. 2012). In contrast, our results have shown that elevated levels of R loops at rDNA promoters lead to reduced rRNA transcription, suggesting an alternative pathway leading to silencing of rRNA transcription. One mechanism might link R-loop formation with effects on chromatin epigenetic status (Castellano-Pozo et al. 2013; Skourti-Stathaki and Proudfoot 2013; Skourti-Stathaki et al. 2014). In keeping with this, there are two related pathways that are regulated by pRNA and *PAPAS*. pRNAs are stabilized by binding to the nucleolar remodeling complex (NoRC) component TIP5 (Mayer et al. 2008) and form uncharacterized RNA:DNA hybrids at the UCE, which in turn recruits a DNA methyltransferase (DNMT3b) to methylate rDNA and silence rRNA transcription (Grummt 2010; Savić et al. 2014; Wehner et al. 2014). Additionally, *PAPAS* also forms RNA:DNA hybrids at rDNA enhancer regions, guiding the CHD4/NuRD complex to the rDNA promoter to repress transcription (Fig. 8; Zhao et al. 2018).

We propose that the R loops we detected that accumulate over G-rich rDNA promoter regions reflect *PAPAS* and/or pRNA hybrids, and that they are increased by RPA KD. We suggest that the formation or accumulation of these R loops is naturally inhibited by RPA, together with other factors such as SETX and/or RNaseH1 (Chan et al. 2014; Abraham et al. 2020). Cells without RPA exhibit stalled RNAP I associated with R loops upstream of the rRNA start site and decreased levels of rRNA transcription. Sense strand R loops have been shown to promote antisense transcription throughout the genome by forming "promoters" for RNAP II (Tan-Wong et al. 2019). An intriguing possibility consistent with our data is that sense strand R loops might promote antisense *PAPAS* transcription when RPA levels are decreased, leading to reduced rRNA transcription.

RPA also functions in maintaining nucleolar homeostasis by preventing nucleolar disorganization. Nucleolar segregation and formation of nucleolar caps are dynamic processes, and are observed when RNAP I transcription is inactivated; for example, by actinomycin D or Top1/2 inhibition (Louvet et al. 2005; Shav-Tal et al. 2005; Shen et al. 2017; Latonen 2019). We observed that nucleolar structures are segregated and fragmented into smaller size and reduced mass in RPA KD cells, and that these changes are due to R-loop-dependent RNAP I transcriptional inhibition when RPA levels are reduced. Interestingly, we observed comigration of RPA and RNAP I from nucleolar to perinucleolar regions following CPT treatment, again in an R-loop-dependent manner. RNaseH1 and R loops have also been shown to display a similar perinucleolar localization after CPT treatment (Shen et al. 2017). Perinucleolar-localized rDNA loci are commonly transcriptionally inactive and typically accumulate marks of constitutive heterochromatin (Peng and Karpen 2007; Pontvianne et al. 2013; McLeod et al. 2014). Therefore, it is likely that the perinucleolar

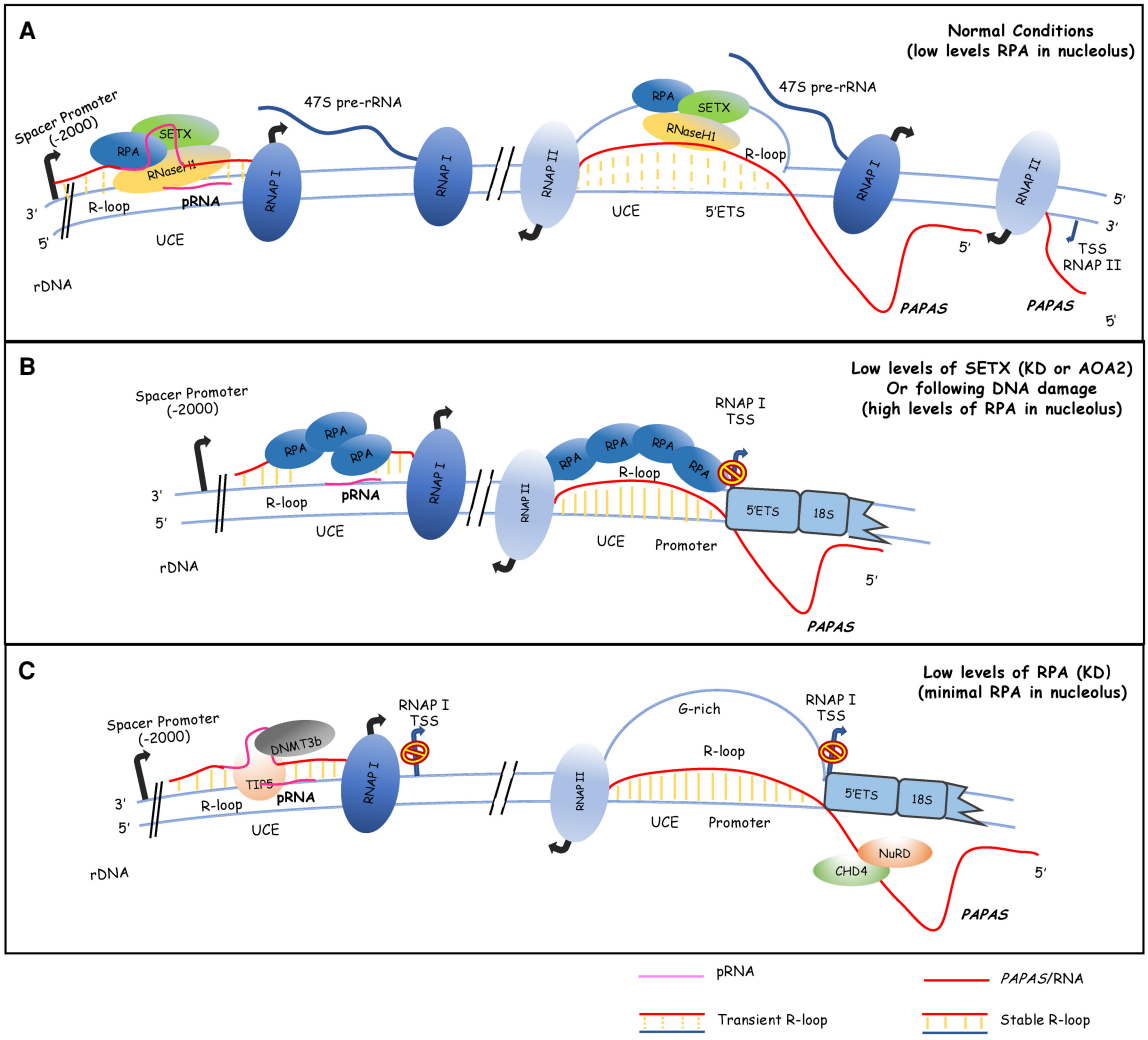

Figure 8. A model for RPA function in combatting nucleolar R loops. (*A*) Under normal conditions, in the presence of RPA, transient R loops formed by pRNA or *PAPAS* transcription are removed by RPA together with RNaseH1, SETX, and perhaps other factors. Positions of rDNA promoter regions and *PAPAS* and pRNA transcripts are shown. Note that portions of two adjacent rDNA loci are illustrated to allow depiction of possible sense pRNA-generated and antisense *PAPAS*-generated R loops over the same regions (e.g., the UCE). Also, it has been suggested that what our data suggest are R loops might be RNA:DNA triplex structures (e.g., Grummt and Langst 2013), and this ambiguity is illustrated with the RNA:DNA hybrid at the *left*. (*B*) In the absence of SETX or the presence of DNA damage, rDNA-associated R loops are stabilized, resulting in excess RPA accumulation. (*C*) In the absence of RPA, RNaseH1 or SETX may not be recruited to rDNA and in any event R loops are stabilized, resulting in increased levels of *PAPAS* and pRNA, which lead to rRNA transcription inhibition, likely through the effects of the *PAPAS*-recruited CHD4/NuRD complex and pRNA-recruited DNMT3b and TIP5.

complexes we observed consist of silenced rDNA loci, perhaps containing R-loop-induced H3K9me2 chromatin marks and repressive HP1 (Skourti-Stathaki et al. 2014), "locked" to the nucleolar periphery (Padeken and Heun 2014). Thus, our results provide evidence that conditions that lead to enhanced formation of R loops and to reduced rRNA transcription, including loss of RPA, result in changes in nucleolar structure and accumulation of silenced R-loop-containing rDNA and associated factors at the nucleolar periphery.

In summary, we have demonstrated a novel role for RPA, functioning to help maintain nucleolar homeostasis in the response to certain stresses, specifically conditions that lead to the formation of excess R loops on rDNA. RPA is directly involved in RNAP I-mediated rRNA transcription, likely by inhibiting *PAPAS* transcription in an R-loop-dependent manner. Importantly, loss of SETX or Top1 results in R-loop-dependent RPA nucleolar accumulation, while RPA depletion results in increased RNAP I levels at upstream rDNA promoter regions, including the UCE, coupled with increased *PAPAS* and pRNA levels and a corresponding decrease of 47S pre-rRNA. Our study not only expands our knowledge of RPA and SETX in nucleolar transcriptional regulation, it also provides insights into their functions in maintaining nucleolar homeostasis under conditions of stress and in human disease.

Materials and methods

Antibodies and drugs

Antibodies recognizing the V5 probe (H-9) (Santa Cruz Biotechnology sc-271926), RNA polymerase I (RPA194 [C-1]) (Santa Cruz Biotechnology sc-48385), fibrillarin (G-8) (Santa Cruz Biotechnology sc-374022), RPA70 (Bethyl A300-241A), RPA32 (Santa Cruz Biotechnology sc-56770), phospho RPA32(S33) (Bethyl A300-246A), GAPDH (Sigma-Aldrich G9545), U2AF65 (Sigma-Aldrich U4758), SETX (Bethyl 301-105A), H3 (Abcam ab8898), phospho-histone H2A.X(Ser139) (Cell Signaling 2577), and topoisomerase I (Bethyl A302-589A-T) were obtained from the indicated suppliers.

Cell culture and generating V5-RNaseH1-expressing stable cells

HeLa cells were from a common laboratory stock and grown in Dulbecco's modified Eagle's medium (DMEM) with 10% fetal bovine serum (FBS). V5-RNaseH1-WT, D210N, and WKKD (W43A, K59A, K60A, and D210N) plasmids were a gift from Xiangdong Fu (University of California at San Diego). For plasmid transfection, 3×10^5 HeLa cells were transfected with 2 μg of each of the above plasmids using Lipofectamine 2000 (Thermo Fisher Scientific). Transfected cells were subjected to hygromycin selection (200 μg/mL) 2 d after transfection for 24 h, and polyclonal cells were then cultured with hygromycin at 100 μg/mL. In experiments with GFP-RNaseH1 plasmids, 2 μg of plasmid was transfected into HeLa cells after siRNA KD for 48 h, and then cells were harvested after an additional 24 h and analyzed by IF.

siRNA transfection and Western blots

HeLa cells and WT/D210N HeLa cells were transfected with the siRNA control NC (TTCTCCGAACGTGTCACGT), si*SETX* (AGCAAGAGAUGAAUUGCCA), si*SETX2* (GCCAGAUCGU AUACAAUUA), or siTop1 (GACAAGAUCCGGAACCAGU) for 72 h at 20 nM with RNAiMAX (Invitrogen 13778), and siRPA70 (AACACUCUAUCCUCUUUCAUGUU), siRPA32 (GCACCUUCUCAAGCCGAAA), and siRPA32-2(GGAAGUAG GUUUCAUCUAU) for 72 h at 10 nM with RNAiMAX. Protein samples were collected by 2× sample loading buffer and were separated by SDS-PAGE. Proteins were transferred to a nitrocellulose membrane (Bio-Rad 1620115) according to standard protocols (Richard et al. 2021). Membranes were blocked in 5% milk–PBST blocking buffer for 30 min at room temperature followed by overnight incubation with the primary antibody diluted in protein-free (TBS) blocking buffer (1:1000; Thermo Scientific, 37570), except for GAPDH and H3 (1:10,000). Secondary antibody was added at 1:25,000 for 30 min at room temperature in PBST + 5% milk. Protein bands were detected by chemiluminescence and signals were captured with a ChemiDoc MP imaging system (Bio-Rad). Multiple exposures were performed to ensure signal were in linear range. All protein signals were normalized to GAPDH or H3.

Immunofluorescence

Cells were cultured on glass coverslips coated with 1% gelatin, and prepared following a previously described protocol (Chen et al. 2019). Briefly, cells were fixed with 4% paraformaldehyde for 20 min at 4°C, and then permeabilized with 0.1% Triton X-100 for 20 min. Cells were then washed three times using PBST, following incubation with blocking buffer for 1 h at room temperature. Then cells were incubated with primary antibody anti-RPA70, RPA32-S33p, fibrillarin, or RPA194 (1:500 dilution) for another 2 h at room temperature. To stain for R loops, cells were fixed and permeabilized in ice-cold 100% methanol for 15 min at −20°C. After washing with PBS three times, cells were incubated with S9.6 antibody (1:2000). After washing, cells were incubated with the appropriate secondary fluorescence-conjugated antibody (Alexa Fluor 488 goat antirabbit IgG or Alexa Fluor 568 goat antimouse IgG; 1:500 dilution; Thermo Fisher) diluted with blocking buffer for 1 h at room temperature. Cells were mounted on slides with mounting buffer containing DAPI (Thermo Fisher) for imaging using a Zeiss Zen confocal microscope 700 with 63× oil objective. Images were recorded with the same settings. Image quantification was performed using ImageJ.

5-fluorouridine labeling nascent RNA

Cells grown on coverslips after siRNA KD for 72 h were incubated with 0.5 mg/mL 5-fluorouridne (FUrd) for 20 min before fixation with 4% paraformaldehyde and permeabilization with 0.5% Triton X-100. Then cells were incubated in blocking buffer for 1 h at room temperature, followed with anti-BrdU antibody to visualize FUrd-labeled RNA using the same IF procedure described above. Signals within the nucleolus were quantified as above.

RPA32 ChIP and V5-RNaseH1 ChIP-qPCR

RPA32 ChIP and R-ChIP-qPCR experiments were performed with cells expressing V5-RNaseH1-WT/D210N/WKKD mutant protein using a standard ChIP protocol described previously (Chen et al. 2019) to capture PRA and R loops along the genome. SETX siRNA (20 nM), 10 nM RPA32, or control siRNA was transfected in HeLa cells with RNAimax for 72 h. RPA32, V5, or RNAP I were immunoprecipitated overnight at 4°C with 2 μg of antibodies. DNA was purified using a PCR purification kit (Qiagen 28104), and collected by 300 μL of elution buffer. qPCR reactions were set up by mixing 3 μL of precipitated DNA with Power SYBR Green PCR master mix (Thermo Fisher Scientific 2008602) and performed using the StepsOnePlus real-time PCR system (Thermo Fisher).

RT-qPCR

RNA extraction was carried out with Trizol (Thermo Fisher Scientific 15596026) followed by DNase I treatment (NEB M0303S). Real-time PCR was performed in 96-well plates with power SYBR Green using StepOnePlus (Applied Biosystems 4367659). cDNA was reverse-transcribed with Maxima reverse transcriptase (Thermo Fisher Scientific EP0741) and a random hexamer (Thermo Fisher Scientific SO142), or strand-specific PCR was performed using corresponding primers. Briefly, PCR reactions were denatured for 10 min at 95°C and 40 cycles of PCR were then conducted for 15 sec at 95°C and for 60 sec at 60°C for each cycle. Signals obtained from each immunoprecipitation are expressed as a percent of the total input chromatin, and then normalized to negative control. All probes used for qPCR in this study are listed in Supplemental Table S1.

Quantification and statistical analysis

ChIP-qPCR data and WB data are shown as mean ± SE based on at least three independent experiments. IF data are shown as box plots with the first and third quartiles as the lower and upper boundaries of the box, with the median shown as the middle line, and with the furthest observation as the end of whisker based on three independent experiments, >150 cells in total. The asterisks ($P < 0.05$ [*], $P < 0.01$ [**], and for $P < 0.001$ [***])

represent the significance of difference between different groups of data based on unpaired Student's *t*-test. All detailed statistical parameters are reported in the figures and the figure legends.

Competing interest statement

The authors declare no competing interests.

Acknowledgments

We thank Xiangdong Fu for generously sharing V5-RNaseH1 plasmids, and Robert Crouch for the GFP-RNaseH1 plasmid. S.F. thanks Patricia Richard for advice and encouragement during the early stages of this project, and Lizhi Liu for proofreading drafts of the manuscript and for support. This work was supported by National Institutes of Health grant R35 GM118136.

Author contributions: S.F. designed all of the work, analyses, and interpretation of all results. S.F. drafted the manuscript and revised it under J.L.M.'s supervision.

References

Abraham KJ, Khosraviani N, Chan JNY, Gorthi A, Samman A, Zhao DY, Wang M, Bokros M, Vidya E, Ostrowski LA, et al. 2020. Nucleolar RNA polymerase II drives ribosome biogenesis. *Nature* **585:** 298–302. doi:10.1038/s41586-020-2497-0

Aguilera A, Gómez-González B. 2008. Genome instability: a mechanistic view of its causes and consequences. *Nat Rev Genet* **9:** 204–217. doi:10.1038/nrg2268

Becherel OJ, Yeo AJ, Stellati A, Heng EY, Luff J, Suraweera AM, Woods R, Fleming J, Carrie D, McKinney K, et al. 2013. Senataxin plays an essential role with DNA damage response proteins in meiotic recombination and gene silencing. *PLoS Genet* **9:** e1003435. doi:10.1371/journal.pgen.1003435

Bhatia V, Barroso SI, García-Rubio ML, Tumini E, Herrera-Moyano E, Aguilera A. 2014. BRCA2 prevents R-loop accumulation and associates with TREX-2 mRNA export factor PCID2. *Nature* **511:** 362–365. doi:10.1038/nature13374

Bierhoff H, Schmitz K, Maass F, Ye J, Grummt I. 2010. Noncoding transcripts in sense and antisense orientation regulate the epigenetic state of ribosomal RNA genes. *Cold Spring Harb Symp Quant Biol* **75:** 357–364. doi:10.1101/sqb.2010.75.060

Bywater MJ, Poortinga G, Sanij E, Hein N, Peck A, Cullinane C, Wall M, Cluse L, Drygin D, Anderes K, et al. 2012. Inhibition of RNA polymerase I as a therapeutic strategy to promote cancer-specific activation of p53. *Cancer Cell* **22:** 51–65. doi:10.1016/j.ccr.2012.05.019

Castellano-Pozo M, Santos-Pereira JM, Rondón AG, Barroso S, Andújar E, Pérez-Alegre M, García-Muse T, Aguilera A. 2013. R loops are linked to histone H3 S10 phosphorylation and chromatin condensation. *Mol Cell* **52:** 583–590. doi:10.1016/j.molcel.2013.10.006

Chan YA, Aristizabal MJ, Lu PY, Luo Z, Hamza A, Kobor MS, Stirling PC, Hieter P. 2014. Genome-wide profiling of yeast DNA:RNA hybrid prone sites with DRIP-chip. *PLoS Genet* **10:** e1004288. doi:10.1371/journal.pgen.1004288

Chen L, Chen JY, Zhang X, Gu Y, Xiao R, Shao C, Tang P, Qian H, Luo D, Li H, et al. 2017. R-ChIP using inactive RNase H reveals dynamic coupling of R-loops with transcriptional pausing at gene promoters. *Mol Cell* **68:** 745–757.e5. doi:10.1016/j.molcel.2017.10.008

Chen JY, Zhang X, Fu XD, Chen L. 2019. R-ChIP for genome-wide mapping of R-loops by using catalytically inactive RNASEH1. *Nat Protoc* **14:** 1661–1685. doi:10.1038/s41596-019-0154-6

Christensen MO, Krokowski RM, Barthelmes HU, Hock R, Boege F, Mielke C. 2004. Distinct effects of topoisomerase I and RNA polymerase I inhibitors suggest a dual mechanism of nucleolar/nucleoplasmic partitioning of topoisomerase I. *J Biol Chem* **279:** 21873–21882. doi:10.1074/jbc.M400498200

Cohen S, Puget N, Lin YL, Clouaire T, Aguirrebengoa M, Rocher V, Pasero P, Canitrot Y, Legube G. 2018. Senataxin resolves RNA:DNA hybrids forming at DNA double-strand breaks to prevent translocations. *Nat Commun* **9:** 533. doi:10.1038/s41467-018-02894-w

Cong R, Das S, Ugrinova I, Kumar S, Mongelard F, Wong J, Bouvet P. 2012. Interaction of nucleolin with ribosomal RNA genes and its role in RNA polymerase I transcription. *Nucleic Acids Res* **40:** 9441–9454. doi:10.1093/nar/gks720

Daniels GA, Lieber MR. 1995. RNA:DNA complex formation upon transcription of immunoglobulin switch regions: implications for the mechanism and regulation of class switch recombination. *Nucleic Acids Res* **23:** 5006–5011. doi:10.1093/nar/23.24.5006

Daniely Y, Borowiec JA. 2000. Formation of a complex between nucleolin and replication protein A after cell stress prevents initiation of DNA replication. *J Cell Biol* **149:** 799–810. doi:10.1083/jcb.149.4.799

Drolet M, Phoenix P, Menzel R, Masse E, Liu LF, Crouch RJ. 1995. Overexpression of RNase H partially complements the growth defect of an *Escherichia coli* ΔtopA mutant: R-loop formation is a major problem in the absence of DNA topoisomerase I. *Proc Natl Acad Sci* **92:** 3526–3530. doi:10.1073/pnas.92.8.3526

El Hage A, French SL, Beyer AL, Tollervey D. 2010. Loss of topoisomerase I leads to R-loop-mediated transcriptional blocks during ribosomal RNA synthesis. *Genes Dev* **24:** 1546–1558. doi:10.1101/gad.573310

El Hage A, Webb S, Kerr A, Tollervey D. 2014. Genome-wide distribution of RNA–DNA hybrids identifies RNase H targets in tRNA genes, retrotransposons and mitochondria. *PLoS Genet* **10:** e1004716. doi:10.1371/journal.pgen.1004716

García-Muse T, Aguilera A. 2019. R loops: from physiological to pathological roles. *Cell* **179:** 604–618. doi:10.1016/j.cell.2019.08.055

García-Rubio ML, Pérez-Calero C, Barroso SI, Tumini E, Herrera-Moyano E, Rosado IV, Aguilera A. 2015. The fanconi anemia pathway protects genome integrity from R-loops. *PLoS Genet* **11:** e1005674. doi:10.1371/journal.pgen.1005674

Ginno PA, Lott PL, Christensen HC, Korf I, Chédin F. 2012. R-loop formation is a distinctive characteristic of unmethylated human CpG island promoters. *Mol Cell* **45:** 814–825. doi:10.1016/j.molcel.2012.01.017

Grummt I. 2010. Wisely chosen paths—regulation of rRNA synthesis: delivered on 30 June 2010 at the 35th FEBS congress in gothenburg, Sweden. *FEBS J* **277:** 4626–4639. doi:10.1111/j.1742-4658.2010.07892.x

Grummt I, Längst G. 2013. Epigenetic control of RNA polymerase I transcription in mammalian cells. *Biochim Biophys Acta* **1829:** 393–404. doi:10.1016/j.bbagrm.2012.10.004

Grunseich C, Wang IX, Watts JA, Burdick JT, Guber RD, Zhu Z, Bruzel A, Lanman T, Chen K, Schindler AB, et al. 2018. Senataxin mutation reveals how R-loops promote transcription by blocking DNA methylation at gene promoters. *Mol Cell* **69:** 426–437.e7. doi:10.1016/j.molcel.2017.12.030

Harding SM, Boiarsky JA, Greenberg RA. 2015. ATM dependent silencing links nucleolar chromatin reorganization to DNA

damage recognition. *Cell Rep* **13:** 251–259. doi:10.1016/j.celrep.2015.08.085

Hass CS, Lam K, Wold MS. 2012. Repair-specific functions of replication protein A. *J Biol Chem* **287:** 3908–3918. doi:10.1074/jbc.M111.287441

Hatchi E, Skourti-Stathaki K, Ventz S, Pinello L, Yen A, Kamieniarz-Gdula K, Dimitrov S, Pathania S, McKinney KM, Eaton ML, et al. 2015. BRCA1 recruitment to transcriptional pause sites is required for R-loop-driven DNA damage repair. *Mol Cell* **57:** 636–647. doi:10.1016/j.molcel.2015.01.011

Kim K, Dimitrova DD, Carta KM, Saxena A, Daras M, Borowiec JA. 2005. Novel checkpoint response to genotoxic stress mediated by nucleolin–replication protein A complex formation. *Mol Cell Biol* **25:** 2463–2474. doi:10.1128/MCB.25.6.2463-2474.2005

Koster DA, Palle K, Bot ES, Bjornsti MA, Dekker NH. 2007. Antitumour drugs impede DNA uncoiling by topoisomerase I. *Nature* **448:** 213–217. doi:10.1038/nature05938

Kruhlak M, Crouch EE, Orlov M, Montaño C, Gorski SA, Nussenzweig A, Misteli T, Phair RD, Casellas R. 2007. The ATM repair pathway inhibits RNA polymerase I transcription in response to chromosome breaks. *Nature* **447:** 730–734. doi:10.1038/nature05842

Larsen DH, Stucki M. 2016. Nucleolar responses to DNA double-strand breaks. *Nucleic Acids Res* **44:** 538–544. doi:10.1093/nar/gkv1312

Latonen L. 2019. Phase-to-phase with nucleoli - stress responses, protein aggregation and novel roles of RNA. *Front Cell Neurosci* **13:** 151. doi:10.3389/fncel.2019.00151

Li L, Zou L. 2005. Sensing, signaling, and responding to DNA damage: organization of the checkpoint pathways in mammalian cells. *J Cell Biochem* **94:** 298–306. doi:10.1002/jcb.20355

Li X, Manley JL. 2005. Inactivation of the SR protein splicing factor ASF/SF2 results in genomic instability. *Cell* **122:** 365–378. doi:10.1016/j.cell.2005.06.008

Liu S, Xu Z, Leng H, Zheng P, Yang J, Chen K, Feng J, Li Q. 2017. RPA binds histone H3–H4 and functions in DNA replication-coupled nucleosome assembly. *Science* **355:** 415–420. doi:10.1126/science.aah4712

Louvet E, Junéra HR, Le Panse S, Hernandez-Verdun D. 2005. Dynamics and compartmentation of the nucleolar processing machinery. *Exp Cell Res* **304:** 457–470. doi:10.1016/j.yexcr.2004.11.018

Manzo SG, Hartono SR, Sanz LA, Marinello J, De Biasi S, Cossarizza A, Capranico G, Chedin F. 2018. DNA topoisomerase I differentially modulates R-loops across the human genome. *Genome Biol* **19:** 100. doi:10.1186/s13059-018-1478-1

Maréchal A, Zou L. 2015. RPA-coated single-stranded DNA as a platform for post-translational modifications in the DNA damage response. *Cell Res* **25:** 9–23. doi:10.1038/cr.2014.147

Marinello J, Chillemi G, Bueno S, Manzo SG, Capranico G. 2013. Antisense transcripts enhanced by camptothecin at divergent CpG-island promoters associated with bursts of topoisomerase I-DNA cleavage complex and R-loop formation. *Nucleic Acids Res* **41:** 10110–10123. doi:10.1093/nar/gkt778

Mayer C, Neubert M, Grummt I. 2008. The structure of NoRC-associated RNA is crucial for targeting the chromatin remodelling complex NoRC to the nucleolus. *EMBO Rep* **9:** 774–780. doi:10.1038/embor.2008.109

McLeod T, Abdullahi A, Li M, Brogna S. 2014. Recent studies implicate the nucleolus as the major site of nuclear translation. *Biochem Soc Trans* **42:** 1224–1228. doi:10.1042/BST20140062

Nguyen HD, Yadav T, Giri S, Saez B, Graubert TA, Zou L. 2017. Functions of replication protein a as a sensor of R loops and a regulator of RNaseH1. *Mol Cell* **65:** 832–847.e4. doi:10.1016/j.molcel.2017.01.029

Padeken J, Heun P. 2014. Nucleolus and nuclear periphery: velcro for heterochromatin. *Curr Opin Cell Biol* **28:** 54–60. doi:10.1016/j.ceb.2014.03.001

Peng JC, Karpen GH. 2007. H3k9 methylation and RNA interference regulate nucleolar organization and repeated DNA stability. *Nat Cell Biol* **9:** 25–35. doi:10.1038/ncb1514

Pontvianne F, Blevins T, Chandrasekhara C, Mozgova I, Hassel C, Pontes OM, Tucker S, Mokros P, Muchova V, Fajkus J, et al. 2013. Subnuclear partitioning of rRNA genes between the nucleolus and nucleoplasm reflects alternative epiallelic states. *Genes Dev* **27:** 1545–1550. doi:10.1101/gad.221648.113

Promonet A, Padioleau I, Liu Y, Sanz L, Biernacka A, Schmitz AL, Skrzypczak M, Sarrazin A, Mettling C, Rowicka M, et al. 2020. Topoisomerase 1 prevents replication stress at R-loop-enriched transcription termination sites. *Nat Commun* **11:** 3940. doi:10.1038/s41467-020-17858-2

Richard P, Manley JL. 2017. R loops and links to human disease. *J Mol Biol* **429:** 3168–3180. doi:10.1016/j.jmb.2016.08.031

Richard P, Feng S, Manley JL. 2013. A SUMO-dependent interaction between senataxin and the exosome, disrupted in the neurodegenerative disease AOA2, targets the exosome to sites of transcription-induced DNA damage. *Genes Dev* **27:** 2227–2232. doi:10.1101/gad.224923.113

Richard P, Feng S, Tsai YL, Li W, Rinchetti P, Muhith U, Irizarry-Cole J, Stolz K, Sanz LA, Hartono S, et al. 2021. SETX (senataxin), the helicase mutated in AOA2 and ALS4, functions in autophagy regulation. *Autophagy* **17:** 1889–1906. doi:10.1080/15548627.2020.1796292

Santoro R, Grummt I. 2001. Molecular mechanisms mediating methylation-dependent silencing of ribosomal gene transcription. *Mol Cell* **8:** 719–725. doi:10.1016/S1097-2765(01)00317-3

Santos-Pereira JM, Aguilera A. 2015. R loops: new modulators of genome dynamics and function. *Nat Rev Genet* **16:** 583–597. doi:10.1038/nrg3961

Sanz LA, Hartono SR, Lim YW, Steyaert S, Rajpurkar A, Ginno PA, Xu X, Chédin F. 2016. Prevalent, dynamic, and conserved R-loop structures associate with specific epigenomic signatures in mammals. *Mol Cell* **63:** 167–178. doi:10.1016/j.molcel.2016.05.032

Savić N, Bär D, Leone S, Frommel SC, Weber FA, Vollenweider E, Ferrari E, Ziegler U, Kaech A, Shakhova O, et al. 2014. lncRNA maturation to initiate heterochromatin formation in the nucleolus is required for exit from pluripotency in ESCs. *Cell Stem Cell* **15:** 720–734. doi:10.1016/j.stem.2014.10.005

Schmitz KM, Mayer C, Postepska A, Grummt I. 2010. Interaction of noncoding RNA with the rDNA promoter mediates recruitment of DNMT3b and silencing of rRNA genes. *Genes Dev* **24:** 2264–2269. doi:10.1101/gad.590910

Shav-Tal Y, Blechman J, Darzacq X, Montagna C, Dye BT, Patton JG, Singer RH, Zipori D. 2005. Dynamic sorting of nuclear components into distinct nucleolar caps during transcriptional inhibition. *Mol Biol Cell* **16:** 2395–2413. doi:10.1091/mbc.e04-11-0992

Shen W, Sun H, De Hoyos CL, Bailey JK, Liang XH, Crooke ST. 2017. Dynamic nucleoplasmic and nucleolar localization of mammalian RNase H1 in response to RNAP I transcriptional R-loops. *Nucleic Acids Res* **45:** 10672–10692. doi:10.1093/nar/gkx710

Sikorski TW, Ficarro SB, Holik J, Kim T, Rando OJ, Marto JA, Buratowski S. 2011. Sub1 and RPA associate with RNA

polymerase II at different stages of transcription. *Mol Cell* **44:** 397–409. doi:10.1016/j.molcel.2011.09.013

Skourti-Stathaki K, Proudfoot NJ. 2013. Histone 3 s10 phosphorylation: 'caught in the R loop!'. *Mol Cell* **52:** 470–472. doi:10.1016/j.molcel.2013.11.006

Skourti-Stathaki K, Proudfoot NJ. 2014. A double-edged sword: R loops as threats to genome integrity and powerful regulators of gene expression. *Genes Dev* **28:** 1384–1396. doi:10.1101/gad.242990.114

Skourti-Stathaki K, Proudfoot NJ, Gromak N. 2011. Human senataxin resolves RNA/DNA hybrids formed at transcriptional pause sites to promote Xrn2-dependent termination. *Mol Cell* **42:** 794–805. doi:10.1016/j.molcel.2011.04.026

Skourti-Stathaki K, Kamieniarz-Gdula K, Proudfoot NJ. 2014. R-loops induce repressive chromatin marks over mammalian gene terminators. *Nature* **516:** 436–439. doi:10.1038/nature13787

Sokka M, Rilla K, Miinalainen I, Pospiech H, Syväoja JE. 2015. High levels of TopBP1 induce ATR-dependent shut-down of rRNA transcription and nucleolar segregation. *Nucleic Acids Res* **43:** 4975–4989. doi:10.1093/nar/gkv371

Sollier J, Cimprich KA. 2015. Breaking bad: R-loops and genome integrity. *Trends Cell Biol* **25:** 514–522. doi:10.1016/j.tcb.2015.05.003

Stork CT, Bocek M, Crossley MP, Sollier J, Sanz LA, Chedin F, Swigut T, Cimprich KA. 2016. Co-transcriptional R-loops are the main cause of estrogen-induced DNA damage. *Elife* **5:** e17548. doi:10.7554/eLife.17548

Suraweera A, Becherel OJ, Chen P, Rundle N, Woods R, Nakamura J, Gatei M, Criscuolo C, Filla A, Chessa L, et al. 2007. Senataxin, defective in ataxia oculomotor apraxia type 2, is involved in the defense against oxidative DNA damage. *J Cell Biol* **177:** 969–979. doi:10.1083/jcb.200701042

Suraweera A, Lim Y, Woods R, Birrell GW, Nasim T, Becherel OJ, Lavin MF. 2009. Functional role for senataxin, defective in ataxia oculomotor apraxia type 2, in transcriptional regulation. *Hum Mol Genet* **18:** 3384–3396. doi:10.1093/hmg/ddp278

Tan-Wong SM, Dhir S, Proudfoot NJ. 2019. R-loops promote antisense transcription across the mammalian genome. *Mol Cell* **76:** 600–616.e6. doi:10.1016/j.molcel.2019.10.002

Toledo LI, Altmeyer M, Rask MB, Lukas C, Larsen DH, Povlsen LK, Bekker-Jensen S, Mailand N, Bartek J, Lukas J. 2013. ATR prohibits replication catastrophe by preventing global exhaustion of RPA. *Cell* **155:** 1088–1103. doi:10.1016/j.cell.2013.10.043

Toledo L, Neelsen KJ, Lukas J. 2017. Replication catastrophe: when a checkpoint fails because of exhaustion. *Mol Cell* **66:** 735–749. doi:10.1016/j.molcel.2017.05.001

Velichko AK, Petrova NV, Luzhin AV, Strelkova OS, Ovsyannikova N, Kireev II, Petrova NV, Razin SV, Kantidze OL. 2019. Hypoosmotic stress induces R loop formation in nucleoli and ATR/ATM-dependent silencing of nucleolar transcription. *Nucleic Acids Res* **47:** 6811–6825. doi:10.1093/nar/gkz436

Wehner S, Dörrich AK, Ciba P, Wilde A, Marz M. 2014. pRNA: NoRC-associated RNA of rRNA operons. *RNA Biol* **11:** 3–9. doi:10.4161/rna.27448

Wold MS. 1997. Replication protein A: a heterotrimeric, single-stranded DNA-binding protein required for eukaryotic DNA metabolism. *Annu Rev Biochem* **66:** 61–92. doi:10.1146/annurev.biochem.66.1.61

Wu X, Shell SM, Zou Y. 2005. Interaction and colocalization of Rad9/Rad1/Hus1 checkpoint complex with replication protein A in human cells. *Oncogene* **24:** 4728–4735. doi:10.1038/sj.onc.1208674

Xiao J, Bing Z, Xiao G, Guan Y, Luan J. 2020. Long non-coding (lnc)RNA PAPAS overexpression inhibits tumor growth in papillary thyroid carcinoma by downregulating lncRNA HOTTIP. *Oncol Lett* **19:** 2281–2285.

Yu K, Chedin F, Hsieh CL, Wilson TE, Lieber MR. 2003. R-loops at immunoglobulin class switch regions in the chromosomes of stimulated B cells. *Nat Immunol* **4:** 442–451. doi:10.1038/ni919

Yuce O, West SC. 2013. Senataxin, defective in the neurodegenerative disorder ataxia with oculomotor apraxia 2, lies at the interface of transcription and the DNA damage response. *Mol Cell Biol* **33:** 406–417. doi:10.1128/MCB.01195-12

Zhao Z, Dammert MA, Grummt I, Bierhoff H. 2016a. lncRNA-induced nucleosome repositioning reinforces transcriptional repression of rRNA genes upon hypotonic stress. *Cell Rep* **14:** 1876–1882. doi:10.1016/j.celrep.2016.01.073

Zhao Z, Dammert MA, Hoppe S, Bierhoff H, Grummt I. 2016b. Heat shock represses rRNA synthesis by inactivation of TIF-IA and lncRNA-dependent changes in nucleosome positioning. *Nucleic Acids Res* **44:** 8144–8152. doi:10.1093/nar/gkw496

Zhao Z, Sentürk N, Song C, Grummt I. 2018. lncRNA PAPAS tethered to the rDNA enhancer recruits hypophosphorylated CHD4/NuRD to repress rRNA synthesis at elevated temperatures. *Genes Dev* **32:** 836–848. doi:10.1101/gad.311688.118

Zou L, Elledge SJ. 2003. Sensing DNA damage through ATRIP recognition of RPA–ssDNA complexes. *Science* **300:** 1542–1548. doi:10.1126/science.1083430